J|A|C|S
COMMUNICATIONS

Published on Web 10/13/2004

Versatile Organic (Fullerene)−Inorganic (CdTe Nanoparticle) Nanoensembles

Dirk M. Guldi,*,†,|| Israel Zilbermann,† Greg Anderson,† Nicholas A Kotov,*,‡ Nikos Tagmatarchis,§ and Maurizio Prato*,§

Institute for Physical Chemistry, Friedrich-Alexander-Universität, Erlangen-Nürnberg, 91058 Erlangen, Germany, Radiation Laboratory, University of Notre Dame, Notre Dame, Indiana 46556, Department of Chemical Engineering and Departments of Materials Science and Biomedical Engineering, University of Michigan, Ann Arbor, Michigan 48109, and Dipartimento di Scienze Farmaceutiche, Università di Trieste, Piazzale Europa 1, 34127 Trieste, Italy

Received April 4, 2004; E-mail: Guldi.1@nd.edu

There is considerable interest in preparing, shaping, and improving building blocks of molecular scale to match the ever-growing demand for multifunctional nanoarchitectures.[1] The spatial organization of dissimilar and otherwise incompatible components in hybrid materials produces a wealth of novel structural features, physical properties, and complex function, which arise from the synergetic interactions of the individual constituents.

Organic/inorganic mixed nanocomposites promise to be valuable to solar energy conversion, photovoltaics, and catalytic reactivity, specifically to novel chemical- and light-driven systems.[2] Despite the prominent features of fullerenes within the context of light-induced charge separation and solar-energy conversion, fullerene-based mixed nanocomposites of well-defined composition and stoichiometry have not been adequately studied.[3] One of the major setbacks, which holds back significant advances in this area, is the insufficient solubility of nanocomposites that carry more than a single C_{60} component and the lack of control over their production.

Harnessing the potential of organic/inorganic mixed nanocomposites required to fine tune the size, topology, and spatial assembly of the contributing parts. In the current work, we report on the use of electrostatic interactions as a versatile means to bind two water-soluble C_{60} derivatives (**C_{60}**) to size-quantized CdTe nanoparticles (**NP**). The advantage of the electrostatic approach, as summarized in this contribution, is (i) the control over the ensemble composition in solution and (ii) favorable electron-transfer behavior in solution (i.e., stable radical ion pairs).

For the current work three different size-quantized **NP** were synthesized with either L-cysteine or thioglycolic acid as surface stabilizers. In particular, green (2.4 nm), yellow (3.4 nm), and red (5.0 nm) **NP**, whose syntheses were carried out following well-known protocols,[4] were examined. To fine-tune the **NP** (photoexcited-state electron donor)/**C_{60}** (electron acceptor) interactions, two regioisomeric bis-adducts, that is, *trans*-2 and *trans*-3 isomers—see Scheme 1, only *trans*-3 isomer shown—were chosen.[5]

The **NP** revealed size-dependent luminescence with maxima at 545, 595, and 616 nm, with lifetimes of 22 ± 1 (red), 21 ± 1 (orange), and 8 ± 1 (green) μs[6] and quantum yields of 15−30%.[7] The strong luminescence is ideally suited for performing fluorescence titration assays, that is **NP** emission at variable **C_{60}** concentrations (between 0 and 1.0×10^{-4} M), also because the luminescence features of **NP** are distinctly different from those of **C_{60}**. In a typical assay the luminescence of **NP** shifts to shorter wavelengths despite the changes in morphology (vide infra) and is quenched in a nonlinear fashion. An example is given in Figure 1 for the red **NP** with *trans*-3 **C_{60}**. This speaks for strong electronic coupling in **NP·C_{60}**. When **C_{60}** is present, a short-lived emission component, which relates to the static quenching event in **NP·C_{60}**, appears with a time constant of ∼100 ps in all samples that contained **NP** and **C_{60}**. Addition of acid induces protonation of the stabilizer component, thus restoring the original **NP** fluorescence intensity. Analogously, titration experiments with a 1.7×10^{-6} M solution of red **NP** and a C_{60} derivative that carries four negative groups led to no fluorescence quenching.

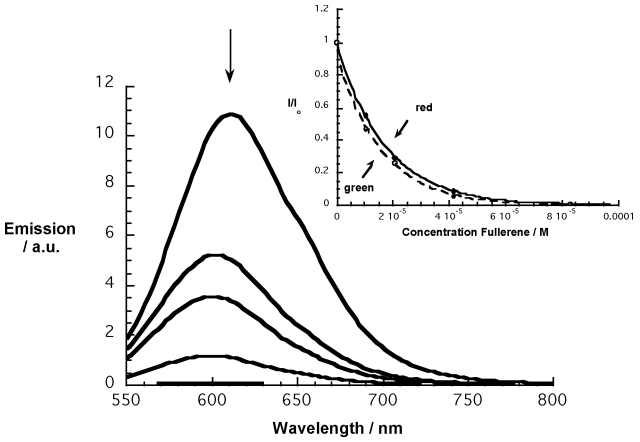

Figure 1. Steady-state emission spectra (λ_{exc} = 500 nm) of red **NP** (1.7×10^{-6} M) and variable concentration of *trans*-3 **C_{60}** (0, 1.04×10^{-5} M, 2.08×10^{-5} M, 4.17×10^{-5} M, and 8.33×10^{-5} M) in H_2O at room temperature—pH 10.1. Insert depicts I/I_0 vs quencher concentration.

Scheme 1. Structure of the Compounds Used in This Work

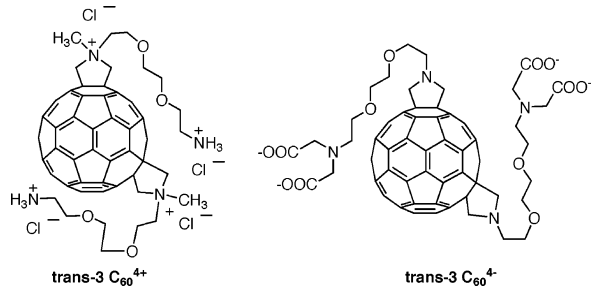

The decrease of emission intensity in **NP** and the short-lived emissive component, is most likely caused by the quenching of photoexcited **NP** through charge transfer to the electron-accepting **C_{60}**—see below—that is bound to **NP**.

† University of Notre Dame.
‡ University of Michigan.
§ Università di Trieste.
|| Friedrich-Alexander-Universität.

10.1021/ja048065f CCC: $27.50

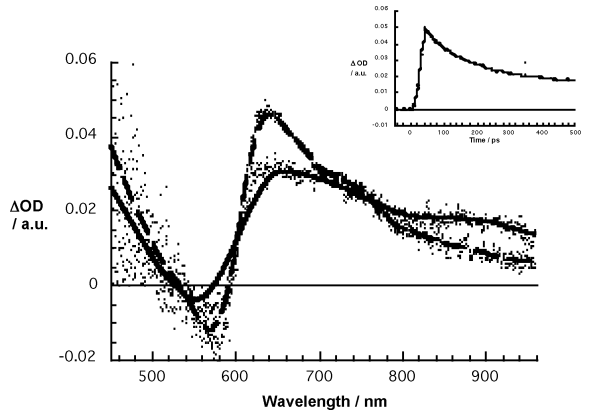

Figure 2. Transient absorption spectrum (vis and NIR part) of red **NP** (1.7×10^{-6} M) in the absence (- - -) and presence of *trans*-2 $\mathbf{C_{60}}$ (ca. 1.0×10^{-5} M) (−−)—recorded 100 ps following a 20 ps laser pulse (λ_{exc} = 532 nm)—showing the characteristic $C_{60}^{\bullet-}$ fingerprint with λ_{max} at 900 nm and bleaching of the oxidized **NP**. (Inset) Charge separation kinetics as recorded at 600 nm.

Furthermore, from plots of I/I_0 versus quencher concentration—see inset of Figure 1—and fitting the I/I_0 versus $\mathbf{C_{60}}$ titration curves to the following procedure:[8]

$$I = I_0 + \frac{\Delta I}{2S_0}[K_{diss} + X + S_0 - \sqrt{(K_{diss} + X + S_0)^2 - 4XS_0}]$$

association constants were calculated that are on the order of $1 \pm 0.5 \times 10^5$ M^{-1} for the red and orange **NP**. A slightly higher value ($4 \pm 0.5 \times 10^5$ M^{-1}), however, was determined for the green **NP**. In summary, electrostatic binding of $\mathbf{C_{60}}$ to **NP** leads to fairly strong complexes with presumably a 1:1 stoichiometry, in which the photoexcited **NP** are subject to rapid electron-transfer deactivation (see below).

To confirm that the product of the intracomplex quenching is indeed charge injection of a conduction band electron of the photoexcited **NP** to the surface-bound $\mathbf{C_{60}}$ we complemented our studies by time-resolved transient absorption spectroscopic measurements with **NP** and **NP·C$_{60}$** following picosecond (i.e., 20 ps) and nanosecond (i.e., 8 ns) pulses. In particular, we see that the photoexcited **NP**, which in a reference experiment decays to the ground state with a monoexponential rate law ($3.8 \pm 0.4 \times 10^7$ s^{-1}), transforms in the presence of $\mathbf{C_{60}}$ (i.e., **NP·C$_{60}$**) nearly instantaneously into a charge-separated radical ion pair. Figure 2 shows the transients recorded for **NP** and **NP·C$_{60}$** with a 100 ps time delay. The intracomposite rate for this fast charge injection with the red **NP** is $7.6 \pm 0.6 \times 10^9$ s^{-1}. Spectroscopic evidence for the radical ion pair is based on (i) transient bleaching in the range where the band-gap transition is located and (ii) the fullerene radical anion ($C_{60}^{\bullet-}$) fingerprint, which depending on the derivative employed maximizes either around 900 nm (i.e., *trans*-2) or 1000 nm (i.e., *trans*-3).[9]

From the absorption time profiles at the $C_{60}^{\bullet-}$ absorption (Figures S1 and S2), we see that the radical ion pair is quite stable on a time scale of up to several hundred microseconds, and we determine a lifetime of 1.5 ± 0.5 ms! Either the facile corrosion of the **NP** or the reducing features of the L-cysteine/thioglycolic acid stabilizer are responsible for the stability. Working with stable **NP·C$_{60}$** suspensions necessitates maintaining an alkaline pH (∼10), which is, in turn, beneficial in suppressing the protonation of $C_{60}^{\bullet-}$ to form $C_{60}H^{\bullet}$ (3.9×10^4 $M^{-1}s^{-1}$).[9]

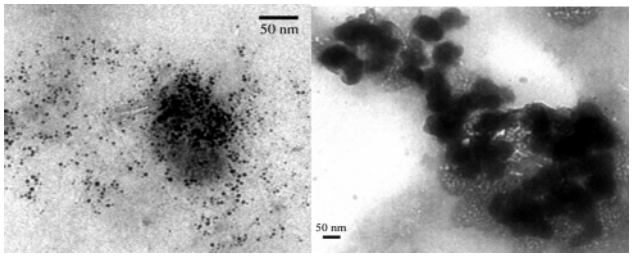

Figure 3. TEM images of red **NP** (∼10^{-5} M)—left image—and **NP·C$_{60}$** (i.e., 10^{-5} M **NP** and 10^{-4} M $\mathbf{C_{60}}$)—right image.

The association constant (i.e., $1 \pm 0.5 \times 10^5$ M^{-1}) between **NP** and $\mathbf{C_{60}}$ in solution, was confirmed by transmission electron microscopy (TEM).[10] Since $\mathbf{C_{60}}$ is soluble in aqueous media and does not aggregate,[5] single molecule are not easily seen in low-resolution TEM. TEM images of red **NP** (∼10^{-5} M) alone are characteristic of uniformly shaped spheres, with a mean size of 6 ± 1 nm—see Figure 3a. When analyzing the **NP·C$_{60}$** composite (i.e., 10^{-5} M **NP** and 10^{-4} M $\mathbf{C_{60}}$) a nanometer-sized pattern of larger objects is seen. As can be observed in Figure 3b the mean size of 60 ± 10 nm exceeds that of **NP**, which can be attributed to the presence of $\mathbf{C_{60}}$. Multiple aggregates can possibly form, which would involve more than one **NP** unit.

In summary, electrostatic binding of $\mathbf{C_{60}}$ to **NP** facilitates the rapid photoinduced electron transfer. The versatility of nanoparticle chemistry opens the exciting possibilities for further engineering of the redox processes in solution and on the electrodes.

Acknowledgment. This work was carried out with partial support from the EU (RTN network "WONDERFULL"), MIUR (PRIN 2002, prot. 2002032171), SFB 583, and the Office of Basic Energy Sciences of the U.S. Department of Energy. This is document NDRL-4558 from the Notre Dame Radiation Laboratory. I.Z. acknowledges sabbatical leave from the Nuclear Research Center Negev, Beer Sheva, Israel.

References

(1) Mirkin, C. A. *MRS Bull.* **2001**, *26*, 535; Kotov, N. A. *MRS Bull.* **2001**, *26*, 992; Coelfen, H.; Mann, S. *Angew. Chem., Int. Ed.* **2003**, *42*, 2350.
(2) Pelizzetti, E.; Schiavello, M. *Photochemical Conversion and Storage of Solar Energy*; Kluwer: Dordrecht, 1997; Fendler, J. H.; Dekany, I. *Nanoparticles in Solids and Solutions*; Kluwer: Dordrecht, 1996; Kamat, P. V.; Meisel, D. *Semiconductor Nanoclusters*; Elsevier: Amsterdam, 1997; Fendler, J. H. *Nanoparticle and Nanostructured Films*; Wiley-VCH: Weinheim, 1998.
(3) Xu, C. M.; Xi, B.; Li, L. Y.; Wang, C.; Wang, S.; Shi, Z. Q.; Fang, J. H.; Xiao, S. X.; Zhu, D. B. *New J. Chem.* **2001**, *25*, 1191; Fujihara, H.; Nakai, H.; *Langmuir* **2001**, *17*, 6393; Sudeep, P. K.; Ipe, B. I.; Thomas, K. G.; George, M. V.; Barazzouk, S.; Hotchandani, S.; Kamat, P. V. *Nano Lett.* **2002**, *2*, 29; Shon, Y. S.; Choo, H. *Chem. Commun.* **2002**, 2560.
(4) Rogach, A. L.; Katsikas, L.; Kornowski, A.; Su, D.; Eychmueller, A.; Weller, H. *Ber. Bunsen-Ges.* **1996**, *100*, 1772.
(5) Bosi, S.; Feruglio, L.; Milic, D.; Prato, M. *Eur. J. Org. Chem.* **2003**, 4741).
(6) Bruchez, M.; Moronne, M.; Gin, P.; Weiss, S.; Alivisatos, A. P. *Science* **1998**, *281*, 2013; Bawendi, M. G. *Solid State Commun.* **1998**, *107*, 709; Mamedova, N. N.; Kotov, N. A.; Rogach, A. L.; Studer, J. *Nano Lett.* **2001**, *1*, 281. Wang, S.; Mamedova, N.; Kotov, N. A.; Chen, W.; Studer, J. *Nano Letters* **2002**, *2*, 817.
(7) An additional minor component was also seen.
(8) Famigni, L.; Johnston, M. B. *New. J. Chem.* **2001**, *25*, 1368. X and S_0 are the titrant ($\mathbf{C_{60}}$) and substrate (**NP**) concentrations, respectively.
(9) For studies on this type of derivatives as electron acceptors, see: Carano, M.; Da Ros, T.; Fanti, M.; Kordatos, K.; Marcaccio, M.; Paolucci, F.; Prato, M.; Roffia, S.; Zerbetto, F. *J. Am. Chem. Soc.* **2003**, *125*, 7139; Guldi, D. M. *J. Phys. Chem. B* **2000**, *104*, 1483.
(10) One drop from the aqueous solution of **NP** (or $\mathbf{C_{60}}$ or **NP·C$_{60}$**) was put to a copper grid (3 mm, 200 mesh) coated with Formvar film. After drying, TEM images were recorded on a Philips TEM 208 at an accelerating voltage of 100 kV.

JA048065F